

## Measurement of residual stresses in surrogate coated nuclear fuel particles using ring-core focussed ion beam digital image correlation

Alexander J. Leide<sup>a,b</sup>, Thomas A. Haynes<sup>c</sup>, Nassia Tzelepi<sup>d</sup>, John Payne<sup>d</sup>, Matthew Jordan<sup>d</sup>, Steven Knol<sup>e</sup>, Jan A. Vreeling<sup>e</sup>, Mark Davies<sup>f</sup>, David T. Goddard<sup>g</sup>, Manuel J. Pfeifenberger<sup>h</sup>, Markus Alfreider<sup>h</sup>, Daniel Kiener<sup>h</sup>, Dong Liu<sup>a,\*</sup>

<sup>a</sup> School of Physics, University of Bristol, Tyndall Avenue, Bristol BS8 1TL, UK

<sup>b</sup> UK Atomic Energy Authority, Culham Science Centre, Abingdon OX14 3DB, UK

<sup>c</sup> School of Engineering, University of East Anglia, Norwich Research Park, Norwich, Norfolk NR4 7TJ, United Kingdom

<sup>d</sup> National Nuclear Laboratory, Central Laboratory, Sellafield CA20 1PG, UK

<sup>e</sup> NRG, Petten, the Netherlands

<sup>f</sup> Ultra Safe Nuclear Corporation, Seattle, USA

<sup>g</sup> National Nuclear Laboratory, Preston Laboratory, Springfields, Preston PR4 0XJ, UK

<sup>h</sup> Chair of Materials Physics, Department of Materials Science, Montanuniversität, Leoben, Austria

### ARTICLE INFO

#### Keywords:

TRISO  
Residual stresses  
FIB-DIC  
PyC  
SiC

### ABSTRACT

Coated fuel particles, most commonly tri-structural isotropic (TRISO), are intended for application in several designs of advanced nuclear reactors. A complete understanding of the residual stresses and local properties of these particles through their entire lifecycle is required to inform fuel element manufacturing, reactor operation, accident scenarios, and reprocessing. However, there is very little experimental data available in the literature on the magnitude of residual stresses in the individual coating layers of these particles. This work applies ring-core focussed ion beam milling combined with digital image correlation analysis (FIB-DIC) to cross-sections of TRISO and pyrolytic carbon coatings in surrogate coated fuel particles to evaluate the residual stresses. Tensile residual hoop stresses are identified in both pyrolytic carbon layers, while silicon carbide experiences a compressive residual hoop stress. Note that these residual stresses, which were not accounted for in the models reported in open literature, have magnitudes comparable to the stresses predicted to arise in real fuel particles during service. A 2D linear-elastic continuum-based finite element analysis has been conducted to investigate the stress relaxation phenomena caused by sectioning stressed coatings on spherical particles. The FIB-DIC method established here is independent of radiation defects and can be applied to irradiated TRISO particles to retrieve first-hand information regarding the residual stress evolution during service.

### 1. Introduction

The concept of applying a coating to nuclear fuel particles to retain fission products first appeared in the 1950 s in the Dragon experimental high temperature gas cooled reactor project [1]. These coatings developed from a single anisotropic “laminar” pyrolytic carbon (PyC) coating, followed by a two-layer “BISO” structure consisting of porous PyC, with an outer dense PyC layer for hermeticity and mechanical structure [2]. Finally, a four-layer coating structure with significantly improved fission production retention was developed, called tri-structural isotropic (TRISO). This became the standard design for high

temperature gas cooled reactors and is being considered for licensing in future commercial power stations. Further variations continue to be developed including multi-layer or zirconium carbide coatings intended to further improve fission product containment and mechanical properties, and large-kernel particles to incorporate a higher fraction of fissile material [3,4].

A standard TRISO coated fuel particle consists of a  $\sim 450 \mu\text{m}$  diameter central fuel kernel (normally UCO or  $\text{UO}_2$ ), a  $\sim 100 \mu\text{m}$  porous carbon “buffer” to absorb fission product recoils and allow for volumetric expansion of the kernel,  $\sim 40 \mu\text{m}$  thick dense inner pyrolytic carbon (IPyC),  $\sim 35 \mu\text{m}$  thick dense cubic silicon carbide ( $\beta$ -SiC), and  $\sim$

\* Corresponding author.

E-mail address: [dong.liu@bristol.ac.uk](mailto:dong.liu@bristol.ac.uk) (D. Liu).

<https://doi.org/10.1016/j.nme.2023.101470>

Received 12 April 2022; Received in revised form 17 April 2023; Accepted 30 June 2023

Available online 1 July 2023

2352-1791/© 2023 Published by Elsevier Ltd. This is an open access article under the CC BY-NC-ND license (<http://creativecommons.org/licenses/by-nc-nd/4.0/>).

40  $\mu\text{m}$  thick outer layer of dense pyrolytic carbon (OPyC) [2,5,6]. The dense PyC and SiC layers retain fission products and provide mechanical integrity, acting as a pressure vessel. The individual TRISO particles are consolidated into a spherical or cylindrical fuel element with either a graphite or SiC matrix for use in pebble bed or prismatic reactors [5,7].

Various fuel performance models, from simple one-dimensional spherically symmetric models to those accounting for coating layer debonding and cracking [8–10], have been developed, incorporating nuclear, thermal, and mechanical properties to predict the evolution of TRISO particles as a function of time, neutron dose, or fuel burnup [11–13], and the effect of neighbouring particles when incorporated in a graphite matrix [14]. The mechanical stresses on coating layers evolve during operation as fission gas pressure increases, pyrolytic carbon changes dimensions and creeps, and SiC swells [15–19]. For instance, the shrinkage of PyC layers compresses SiC tangentially, and the PyC layers are correspondingly in tension, assuming the layers remain bonded which is beneficial to prevent particle radial fracture. For an intact particle during service, SiC is predicted to experience a compressive tangential (or hoop) stress peaking around  $-700$  MPa. However, SiC in a particle with cracked IPyC can experience a tensile stress of  $\sim 400$  MPa near the crack tip, approaching the failure stress of SiC [19]. Other models exploring different TRISO design parameters predict lower stresses in the coatings of intact particles. For example, Li *et al.* found that the compressive tangential stress in SiC peaked at less than  $-400$  MPa in most scenarios [15], and when incorporated in a graphite matrix, Boer *et al.* reported that the peak compressive stress in SiC was  $\sim -300$  MPa compared to  $-450$  MPa for an individual TRISO particle [14]. Interface debonding and particle asphericity can also contribute to tensile stresses in SiC and increased failures of TRISO coatings [9,10]. Note that the input material properties to the above models are not necessarily for the specific forms of SiC and PyC found in TRISO coatings; they are often derived from literature irradiation experiments on similar materials such as monolithic bulk CVD SiC and PyCs as summarised in ref [18]. The SiC layer of various forms of TRISO particles is significantly less stiff than bulk CVD SiC, whose elastic modulus is assumed to apply to TRISO SiC in most fuel performance models [20,21]. Accurate material properties must be measured from actual TRISO coatings as inputs for these models.

In addition, the residual stresses in as-manufactured particle coatings have not been considered in the published models; in all recent models the stresses for PyC and SiC layers begin at zero. An early investigation at the UK Atomic Energy Authority compared stresses generated by cooling coated particles prepared at high temperatures using methane as a precursor gas, and lower temperatures using propylene [22]. This work was limited by experimental knowledge at the time and was re-published and updated in 2002, showing that in their model TRISO particles, IPyC experiences 20 MPa tension, SiC  $-57$  MPa compression, and OPyC 15 MPa tension in the tangential direction after cooling from  $1200$  °C to room temperature, caused by differential thermal expansion of SiC and PyC ( $\alpha_{\text{SiC}} = 5 \times 10^{-6} \text{ K}^{-1}$  and  $\alpha_{\text{PyC}} = 5.5 \times 10^{-6} \text{ K}^{-1}$ ,  $\Delta\alpha = -0.5 \times 10^{-6} \text{ K}^{-1}$ ) [10]. Despite calculating this, it was not included in calculations of in-service stress evolution in the same paper, which began again at zero stress. While these processing-induced stresses are small, they are not negligible. Additionally, some of the values used for these calculations such as thermal expansion coefficient and elastic modulus result in lower residual stresses than if other literature values had been used.

A recent investigation of coated particles from the PYCASSO irradiation programme suggested that residual stresses are not only critical for the high temperature ( $1000$  °C) mechanical integrity of the particles, but also potentially impact the dimensional change of the coatings with neutron irradiation [23]. As such, it is of paramount importance to gain experimental insights to the local residual stresses and properties of TRISO coatings to understand its in-reactor behaviour.

### 1.1. Local residual stress characterization

The measurement of TRISO properties remains challenging. Micro-mechanical tests can be used to measure local mechanical properties of coatings [3,20,21,24,25], and crushing experiments can provide information regarding the mechanical strength of complete particles [17,23,26–31]. Reference [21] presents scanning probe microscopy images of indents in the TRISO SiC layer with considerably longer cracks emanating from the indent in the particle's tangential direction than the radial direction. This was attributed to variations in the local micro-structure; however, this crack asymmetry may also be an indicator of non-equibiaxial residual stress in the SiC coating. Residual stresses play an important role in the nanoindentation fracture of silicon carbide [32]. Previously, electron backscatter diffraction (EBSD) was used to estimate residual stress in the SiC coating of TRISO particles based on local crystal misorientation [33–35]. This qualitative visualisation method found that elongated grains had more misoriented pixels than small equiaxed grains. Although local misorientation can indicate the possibility of residual strain, these methods are relative to the reference orientation of that grain and are not an absolute measure of strain in the coating. Further, such measurements can be affected by crystalline defects such as dislocations and stacking faults within the diffracting volume, leading to different conclusions.

Residual stresses can be measured in various ways on an engineering scale, and several are available with microscopic spatial resolution such as Raman spectroscopy and electron or X-ray micro-beam diffraction [36,37]. Raman spectroscopy uses the change in a spectral peak position relative to a stress-free reference, combined with an empirical material-dependent coefficient to determine residual stress [38]. Diffraction methods directly measure crystal lattice spacing, calculate strain compared to a reference, and convert to stress using elastic constants. Both methods rely on comparing a signal to a stress-free reference material with an identical crystal structure, which is not available in all materials. Although a range of coefficients for converting Raman shift to stress are available in the literature for SiC polytypes and carbon [39–45], the technique is not necessarily applicable in the case of the component materials of TRISO which have not been calibrated. Additionally, Raman spectroscopy is normally independent of spatial directions, giving an average signal for the gauge volume with no information regarding the directions of stress. This is adequate if the stress state is known to be hydrostatic (e.g., those environments created in a diamond anvil cell), equibiaxial (e.g., thin films), or uniaxial; however, care must be taken if the stress state is more complex or unknown as in the case of TRISO particles. Additionally, Raman spectroscopy and diffraction are useful techniques for characterising radiation defects [46–48]; however, this can negate their applicability to measuring residual stresses in materials containing radiation or processing defects.

Introducing traction-free surfaces and measuring a geometric relaxation strain is the principle behind several microscopic residual stress evaluation methods. A focussed ion beam (FIB) is used to incrementally remove material, while a scanning electron microscope (SEM) acquires a sequence of images to record the relaxation process. This class of methods is reviewed in ref. [49]. Relaxation displacements can be measured with sub-pixel resolution using digital image correlation (DIC), from which strain can be calculated. Depending on the geometry, a finite element or analytical model may be required to calculate residual stress from relaxation strain [50,51]. Various geometries are available depending on the situation: ring-core, blind hole, slot, 4-slot, and microcantilever [49,52–56]. For this class of methods, no stress-free reference is required; relaxation is to a new equilibrium determined by the geometry of the experiment. This could be a dynamic equilibrium in the case of multi-layer coatings or thin coatings on a substrate, or a complete relaxation where the milling depth is sufficiently deep (depth greater than pillar diameter for ring-core geometry [51]). The ring-core geometry is most versatile as it allows isotropic

stress relief, and has been most widely developed in the literature and through the ISTRESS project led by Università Degli Studi Roma Tre [49,52,57,58].

This work has investigated and applied FIB-DIC, for the first time as far as the authors are aware based on open literature, to the measurement of residual stresses in TRISO coatings. The key experimental points will be summarised and discussed. The relaxation of stresses caused by sectioning the spheres has been investigated by finite-element analysis and the results are consistent with the experimental observations. The method established is independent of radiation defects and can be applied to irradiated TRISO to validate models of material evolution during operation in a reactor.

## 2. Materials, experimental methods and modelling

### 2.1. Materials

Two types of surrogate TRISO fuel particles were used in this work. A sample named “PyC-1” was manufactured by Commissariat à l’Energie Atomique (CEA) as part of the PYrocarbon irradiation for Creep And Swelling/Shrinkage of Objects (PYCASSO) project, and consists of a 1 mm diameter alumina kernel, 250  $\mu\text{m}$  thick porous carbon buffer, and a 40  $\mu\text{m}$  thick PyC coating [4]. The second sample named “USNC” was provided by Ultra Safe Nuclear Corporation and is a TRISO particle embedded in a silicon carbide matrix as a prototype “Fully Ceramic Microencapsulated” (FCM) fuel pellet. The USNC particle consists of a 790  $\mu\text{m}$  diameter zirconia surrogate kernel with a traditional four-layer TRISO coating structure (87  $\mu\text{m}$  buffer, 36  $\mu\text{m}$  IPyC, 40  $\mu\text{m}$  SiC, 32  $\mu\text{m}$  OPyC).

The PYCASSO particles were manufactured specifically for a separate effects irradiation campaign where the effects of fission in the particle kernel are intentionally removed, while the USNC particles are intended for material development purposes in non-radiological laboratories for easier handling. Alumina and zirconia beads are readily available to act as surrogate kernels in coated particles; alumina is beneficial for X-ray imaging in the PYCASSO experimental campaign, while zirconia is more representative of the density and thermal properties of  $\text{UO}_2$  which is useful for fuel manufacturing trials. The as-received properties of the coating layers of surrogate coated particles are expected to be similar to “real” particles containing a uranium-bearing kernel assuming the coating deposition conditions are the same. The major difference is the coefficient of thermal expansion (CTE) of the kernel, however the porous

buffer and debonding between the kernel and buffer should decouple any CTE mismatch-induced mechanical stresses between the kernel and coatings. The effect of irradiation and kernel fission is discussed later in the paper.

The PyC-1 particle was mounted on an SEM stub using silver paint such that it is effectively free-standing. To avoid any unintended material modification or redistribution of residual stresses by mechanical grinding, a system combining a femtosecond laser and a FIB developed at Montanuniversität Leoben was used to cut a cross-section using the femtosecond laser, as introduced in [59]. Laser parameters used were a wavelength of 515 nm, a pulse duration of 500 fs and a fluence of 3.2 J/cm<sup>2</sup>. For details on selection of optimized laser parameters for grazing incident machining, please refer to [60]. Nonetheless, the typical curtaining surface features were unavoidable over such a large focal depth. The cut surface was at  $\sim 80\%$  particle height. The USNC sample was cut from a larger FCM pellet using a diamond saw before mechanical grinding with 220 grit and 1200 grit diamond impregnated resin disks, and polishing with 3  $\mu\text{m}$  and 1  $\mu\text{m}$  diamond suspensions on polishing cloths. As the sample contained many particles, the largest diameter particle was chosen for experimentation, being considered closest to the particle equator. Overviews of these particles are shown in Fig. 1.

### 2.2. Experimental methods

Focused ion beam scanning electron microscopy (FIB-SEM) digital image correlation (DIC) experiments were performed in a FEI Helios Nanolab 600. Periodic surface features from the laser milling process [60] provided suitable surface features for tracking during experiments on PyC-1 (Fig. 2 (a)). The mechanically polished surface of the USNC sample was comparatively featureless, so a random array of platinum spots was deposited using electron beam deposition of a precursor gas in the FIB-SEM (Fig. 2 (b)). Depending on sample requirements, other speckle patterns may be suitable such as a dispersion of nanoparticles, or sputter deposition of gold before surface modification by FIB imaging [52,61].

The sample was aligned such that the x-axis of the image was in the tangential direction of the coating, and the y-axis was aligned with the radial direction (see Fig. 1 and Fig. 2). The fast SEM scan direction (x-axis) is always more reliable in SEM-DIC, and is aligned to the tangential direction which is of most interest for TRISO stress measurements. Examples of y-direction radial results are shown in Figure S5 of supplementary material. The stage was allowed to settle for approximately 15

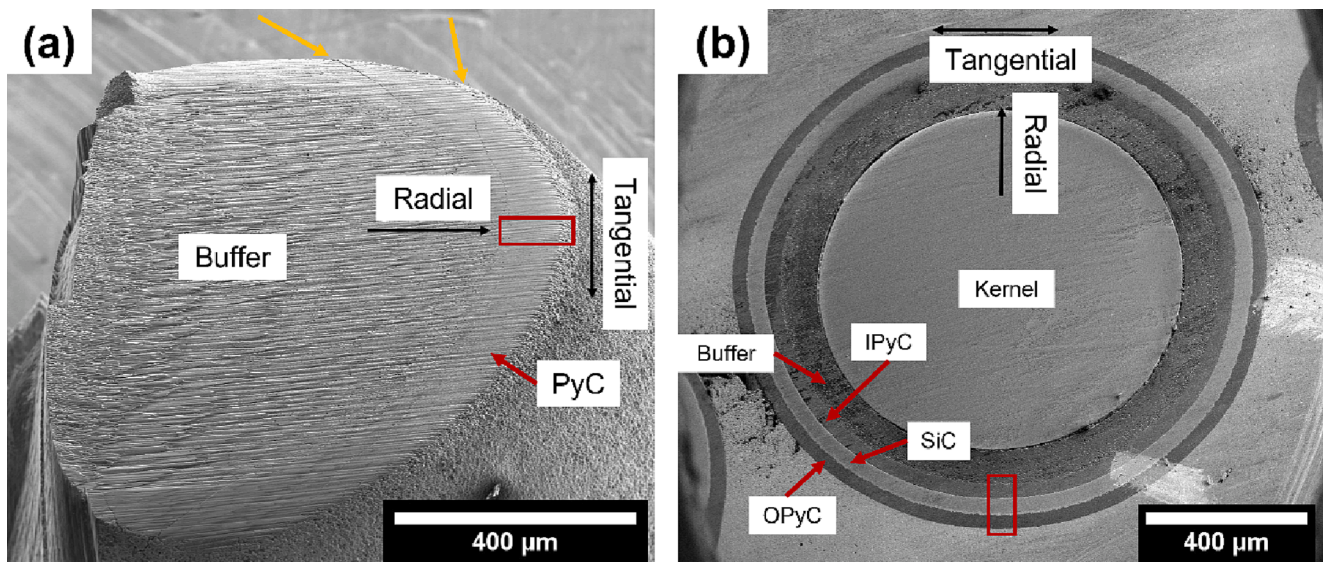
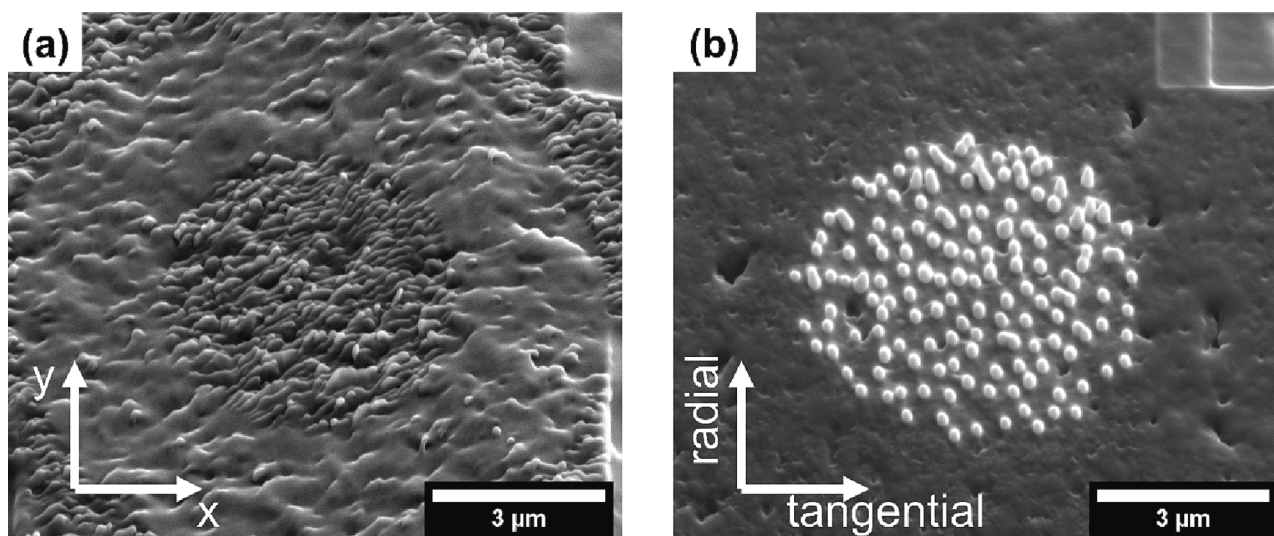


Fig. 1. Overviews of particles studied. (a) PyC-1, (b) USNC. Red boxes indicate the regions where pillars were milled, and orange arrows indicate cracks in the PyC coating of the PyC-1 particle.



**Fig. 2.** Comparison of DIC speckle patterns on pyrolytic carbon. (a) surface features from laser milling on the PyC-1 particle; (b) electron beam deposited platinum dots on the USNC sample. Coordinate arrows show the relationship between x- and y-axes in the images and the tangential and radial directions in the particle coordinate system.

min before beginning the FIB milling. The ring was milled using 30 keV Ga<sup>+</sup> ions at 460 pA current. The outer ring diameter was 7.5 μm with a core diameter of 5 μm. Due to the Gaussian beam profile, the pillars became tapered during milling such that the core became narrower than 5 μm as the experiment proceeded. SEM images were acquired semi-automatically after every 60 s of milling. The electron beam energy was 5 kV with a current of 690 pA and a dwell time of 300 ns. Sixteen images were acquired and averaged for each image step. The scanning area was corrected to account for the 52° stage tilt. Milling proceeded until the pillar height was greater than  $1.5 \times$  the diameter to ensure complete elastic stress relief at the surface of the pillar [51]. This allows direct calculation of residual stress with no need for extrapolation by finite element analysis.

DIC analysis of the image sequences was conducted using the Matlab-based NCORR code [62]. The region of interest (ROI) was an ellipse set in the centre of the speckle pattern on the pillar surface. A border was left between the ROI and pillar edge to account for tapering and stray ion damage during FIB milling. The DIC “subset radius” was 50 pixels, “subset spacing” was 10 pixels, and the “strain radius” for calculating strain from displacement gradients was 5 subsets. The normalised least squares correlation criterion is optimal near zero, and a cut-off was set at 0.25 to remove incorrectly tracked subsets from analysis.

For each image in the sequence, there is a distribution of values for each strain component ( $\epsilon_{xx}$ ,  $\epsilon_{xy}$ ,  $\epsilon_{yy}$ ). These are plotted as a histogram, and a probability distribution curve is fitted (Fig. 3), the peak of which is extracted as the strain relief at the surface of the pillar at that image step. This is intended to minimise the influence of errors in DIC or imaging, and microstructural variations in strain relief which can cause outliers in the strain distribution affecting mean values, while median values are less affected by these factors. Images acquired over ten minutes with no milling and analysed with the same DIC technique were measured with strains less than  $5 \times 10^{-4}$ , which is used as a measure of sensitivity of this technique.

While the relaxation strain is the most appropriate output of FIB-DIC measurements, conversion to stress is useful for understanding the scale of residual stresses and relating to models. Quasistatic nanoindentation was performed using a Hysitron TI Premier nanoindenter with a Berkovich diamond tip. Invalid indentations were removed from the dataset, and reduced modulus was calculated from load-displacement curves using the Oliver-Pharr method, and Young’s modulus calculated based on the Poisson ratio and modulus of the diamond indenter tip [63]. Values were averaged between 500 and 1000 nm, avoiding the small

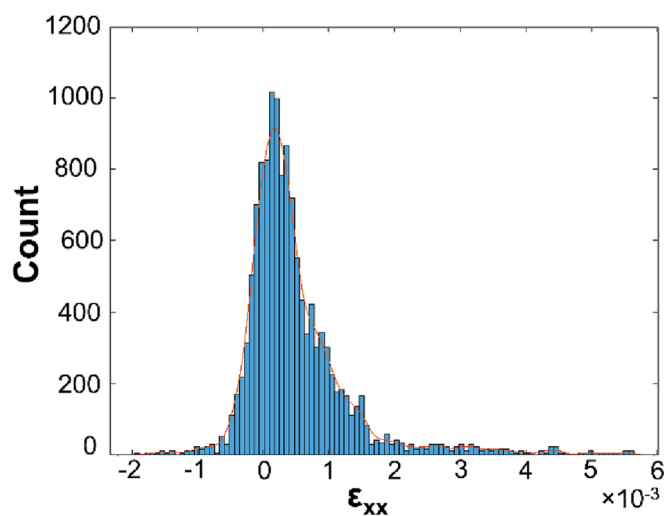


**Fig. 3.** Example strain histogram ( $\epsilon_{xx}$ ) with fitted probability distribution curve.

indentation depth size effect, while being on the length-scale of the micropillars. These values are summarised in Table 1. These values are comparable to nanoindentation experiments in the literature, where lower elastic moduli is related to porosity in the deposited TRISO coatings compared to bulk materials [3,20,21,25].

### 2.3. Finite element analysis

In standard specimen geometries where a flat surface is prepared from a bulk sample, a simple plane stress state can be assumed for near-surface measurements. Residual stresses in cross-sectioned bulk

**Table 1**  
Young’s modulus of TRISO layers measured by nanoindentation.

	USNC	PyC-1
IPyC	$22.4 \pm 0.5$ GPa	$22.1 \pm 0.8$ GPa
SiC	$341.2 \pm 30.1$ GPa	N/A
OPyC	$24.1 \pm 0.9$ GPa	N/A

materials can be calculated using the methodology proposed in reference [64] where the original stress state is unknown but can be back-calculated by the superposition of two complementary experimental measurements. For a hemispherical specimen prepared from spherical particle, the residual stresses in the coating could be relaxed due to the removal of mechanical constraints, which requires further investigation. To investigate if cross-sectioning a coated particle modifies the residual stresses in the particle coating, two axisymmetric finite element models were constructed using Abaqus 2023, representing the PYCASSO and USNC particles. An axis perpendicular to the axis of rotation was identified as the cut axis and a symmetry boundary condition applied; removal of the boundary condition was identified with sectioning. Material properties for the models are shown in Table S1 of supplementary material. In order to carry out a coupled temperature-displacement simulation, ABAQUS requires the density, thermal conductivity and specific heat capacity; these were set to arbitrary values of  $1000 \text{ kg m}^{-3}$ ,  $10 \text{ J m}^{-1} \text{ K}^{-1}$  and  $100 \text{ J kg}^{-1} \text{ K}^{-1}$  respectively. Under the instantaneously isothermal conditions modelled, any differences will not impact the results obtained.

To achieve an arbitrarily stressed particle, the simulations consisted of four coupled temperature-displacement steps, each lasting one hour, during which:

1. The temperature was increased to  $1200 \text{ }^\circ\text{C}$ .
2. The temperature was held at  $1200 \text{ }^\circ\text{C}$  and an arbitrarily high creep rate introduced to equilibrate all stressed.
3. The temperature was reduced to  $20 \text{ }^\circ\text{C}$ .
4. The boundary condition was removed, representing the sectioning of a particle.

The purpose of this finite element modelling is to assess whether cutting an arbitrarily stressed spherical shell causes a stress redistribution, and whether this is likely to impact experimental measurements on cross-sectioned particles. Considering the arbitrary stress which is introduced to the coating, the numbers are illustrative, and the finite element model should be treated as such an approximation.

An alternative simplified modelling approach was also implemented

to explore further variables of stress redistribution caused by cross-sectioning. This is reported in more detail in supplementary material.

### 3. Results

#### 3.1. Free standing PyC-1 particle

Three pillars were prepared in the pyrolytic carbon layer of the PyC-1 sample, and their tangential strain relief curves as a function of image number are shown in Fig. 4. During milling, all three pillars underwent an approximately linear strain relief, until reaching a plateau where complete strain relief is achieved. This plateau refers to the relevant strain for converting to residual stress. All three pillars experience a compressive strain relief, indicating a tensile residual stress in the coating. Using a Young's modulus of  $22.1 \text{ GPa}$ , the average residual stress in the PyC layer is  $\sim 140 \text{ MPa}$ . Pillars a and c have a smaller strain relief than pillar b, possibly due to the presence of the free outer surface and the compliant buffer layer and interfacial crack.

This crack is visible along the buffer-PyC interface, marked with an orange arrow in Fig. 4, despite the non-contact sample preparation method of laser milling. Following the analysis in section 2.3, this is attributed to stress redistribution while sectioning the sphere, as it could not be caused by damage during mechanical sample preparation. Note that these cracks were always at the PyC and buffer interface and propagate into the PyC layer. More images of these cracks are shown in Figure S2 of Supplementary Materials (SM).

#### 3.2. Finite element analysis of PYCASSO particle sectioning

Fig. 5 shows the maximum principal stress prior to and following the removal of the boundary condition along the x-axis for the PYCASSO particle. Following removal of the boundary condition, a significant discontinuity is seen at the kernel-buffer interface. This is the result of the lower elastic modulus in the buffer and stress distribution following release. This tensile discontinuity may cause fracture or debonding between the kernel and buffer which is not the primary focus of the elastic finite element modelling here, but has been captured in previous

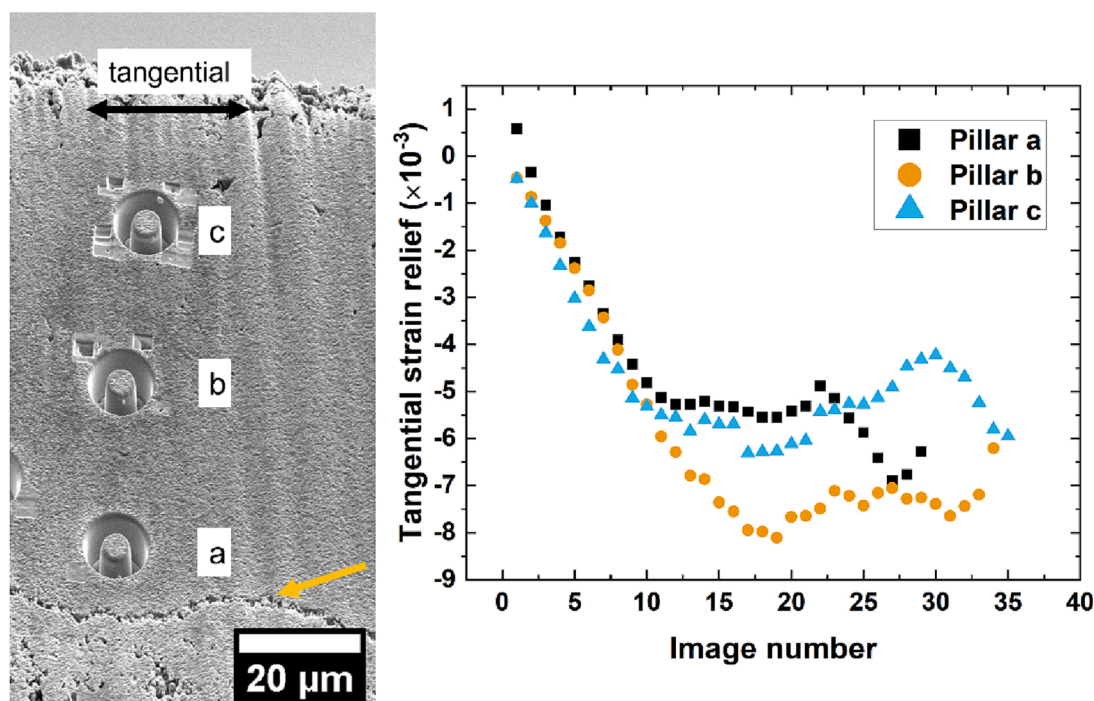


Fig. 4. Three pillars in the pyrolytic carbon coating of sample PyC-1, with their corresponding tangential strain relief curves. An interfacial crack is indicated with the orange arrow.

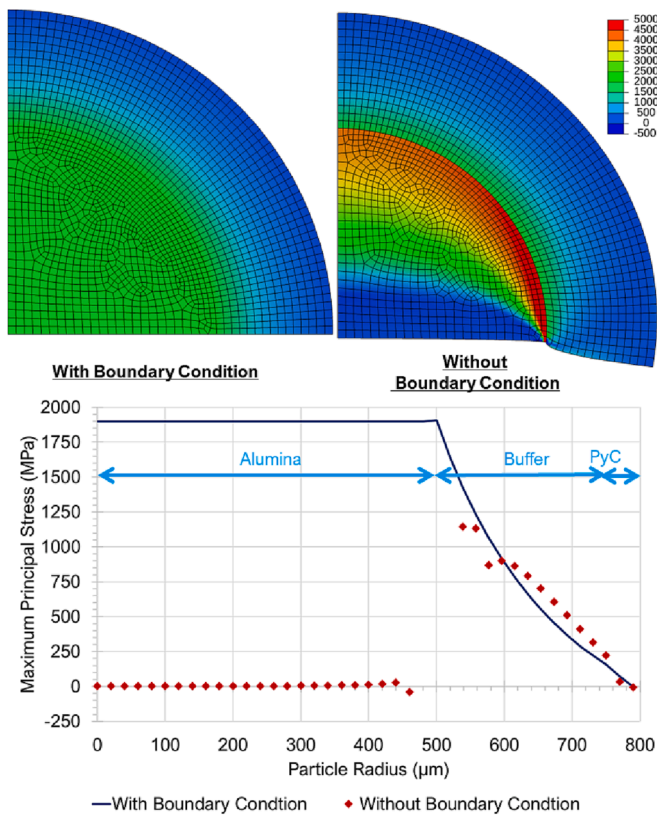


Fig. 5. Maps of the maximum principal stresses in a spherical particle with the boundary condition and in a hemisphere without the boundary condition. The deformation scale is exaggerated in the case without the boundary condition. Graph plots the maximum principal stress as a function of radial position on the surface of the particles.

peridynamic modelling work [65]. The stress in the kernel is effectively reduced to zero following removal of the boundary condition. Beyond 50 μm into the buffer, the stress state becomes similar between the models with and without the boundary condition. To a smaller degree compared to the kernel-buffer discontinuity, there is a step change across the buffer-PyC interface. To reiterate, the values are not expected to be as high in a real particle; stresses of this magnitude are likely to cause microcracking or interfacial debonding.

### 3.3. Constrained USNC particle

In an attempt to restrict radial displacements and minimise the stress redistribution during sectioning which can cause interfacial cracking, a TRISO particle embedded in a stiff silicon carbide matrix was studied. A pillar was made in the centre of each of the IPyC, SiC, and OPyC layers. No cracks are seen at the interfaces between the TRISO layers nor between OPyC and the SiC matrix, however, some brightening is observed due to topological relief and roughness between IPyC and SiC with the tilted stage in the SEM (Fig. 6 (a)). This contrast is only observed at the IPyC – SiC interface and not at the SiC – OPyC interface. This is due to microstructural differences between these interfaces where SiC has grown into IPyC pores; whereas OPyC has grown on a dense SiC and has a smooth interface. Additional pictures of this are shown in Figure S3 and S4 of supplementary material.

IPyC and OPyC both have a compressive relaxation strain indicating a tensile residual stress, while the SiC relaxation strain is tensile indicating compressive residual stress. Using 341 GPa as the stiffness of SiC, 22.4 GPa as the stiffness of IPyC, and 24.1 GPa as the stiffness of OPyC, these relaxation strains correspond to residual tangential (hoop) stresses of approximately –785 MPa in SiC and 78 MPa in IPyC, and 58 MPa in OPyC.

### 3.4. Finite element model of constrained USNC particle

A similar model to the one used for the free standing PYCASSO particle was created to represent a typical TRISO coated particle embedded in a SiC matrix to replicate the experiment described above. Fig. 7 shows the maximum principal stresses in the particle before and after cross-sectioning. Similar to the PYCASSO particle in section 3.2, stress in the kernel is relaxed, and a discontinuity between the kernel and buffer appears due to the significantly differing elastic properties. In this multi-layer coating, there are additional interfaces between the SiC and PyC layers which are discontinuities. Compared to the spherical particle, the PyC layers have similar residual stresses in the cut hemisphere, however, the SiC layers have approximately double the residual stresses. To reiterate, the stresses generated in the model are illustrative rather than those expected to be generated during the real thermal history of the particle.

## 4. Discussion

### 4.1. Residual stresses in TRISO particles

The pyrolytic carbon layer is in residual circumferential tension in both types of particle, with the PyC-1 particle experiencing a slightly

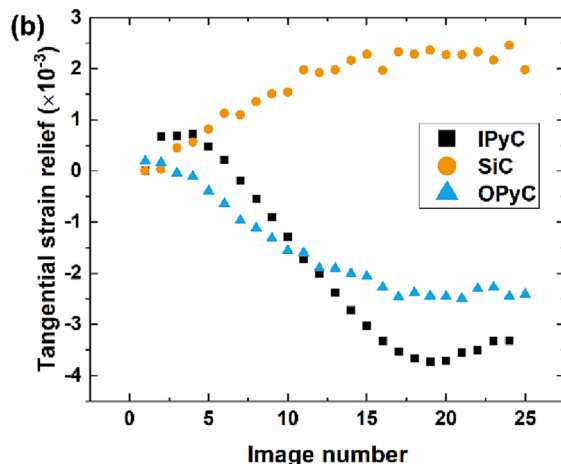
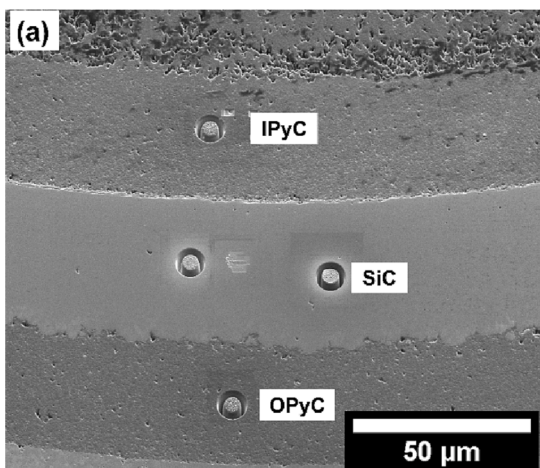


Fig. 6. SEM image of pillars in the USNC pellet. (b) tangential strain relief of the three pillars.

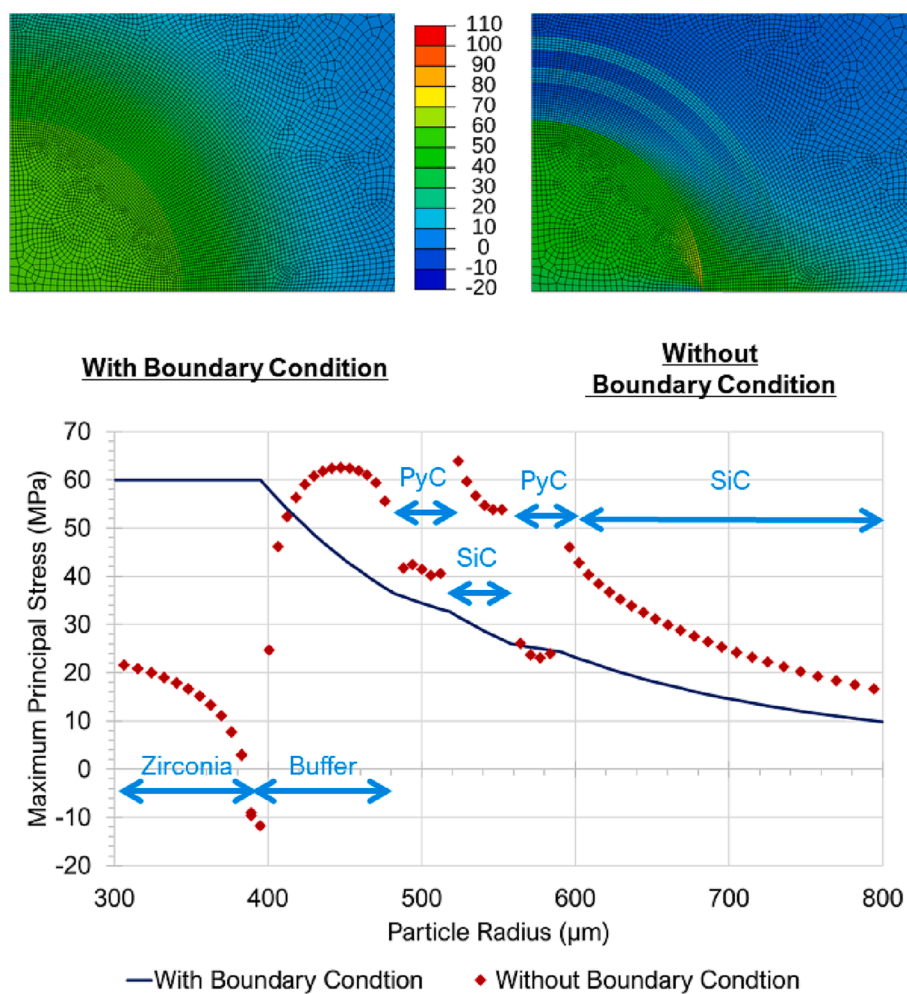


Fig. 7. Maps of maximum principal stress for a spherical and hemispherical TRISO particle in a SiC matrix. The maximum principal stress as a function of radial position along the cross-section is plotted below.

larger magnitude of residual tensile stress than the USNC particle. This is likely to be a combination of factors: the different particle structures, manufacturing conditions and resulting microstructures, hemisectioning stress modification and experimental geometry. The cut surface of the PyC-1 particle is above the equator, which may explain the large tensile circumferential stress which is shown in the supplementary modelling results.

Strain relief curves for PyC-1 show fluctuations in the plateau region after initial strain relief as the trench is milled deeper. This may be due to non-elastic mechanisms of accommodating strain, such as cracking, or by local variations in stiffness due to porosity or partially graphitised carbon. As the trench is milled deeper, the stress relief equilibrium varies as the material is not homogenous as assumed in the criterion for total strain relief at depths greater than the pillar diameter [51]. While there are fluctuations in this plateau region, they are small compared to the total strain relief profile. Similar behaviour is seen for IPyC and OPyC in the USNC sample, including a tensile strain relief in the first six steps of the IPyC experiment.

The SiC layer experiences a small relaxation strain due to the high stiffness of this material. The strain sensitivity of this experimental method is  $\sim 25\%$  of the relaxation strain of the pillar made in the SiC layer of the USNC sample. It is relieved linearly up to the plateau which remains comparatively flat with increasing milling depth. CVD SiC is dense on the length scale of these experiments, without the porosity and complex microstructure of pyrolytic carbon, which may explain its stability once relieved of stress; it can be considered as a homogenous

material with complete strain relief at depths greater than the pillar diameter [51]. A compressive residual stress in SiC is beneficial for TRISO particles as it opposes stresses leading to radial cracking, potentially extending the lifetime of particles in a reactor. Further synergistic effects would need to be investigated, such as the effect this residual stress may have on radiation creep.

The origins of the residual stresses in TRISO coatings are likely to arise from two aspects: (i) the residual stresses introduced by crystal growth during CVD process such as growth twins and stacking faults, and (ii) due to differential contraction during cooling from the CVD processing temperature to room temperature. The former level of residual stress is hard to approximate, however the residual stress induced by differential thermal contraction can be estimated. PyC has a larger coefficient of thermal expansion and lower elastic modulus than SiC, thus contracting more during cooling from the CVD temperature, and compressing the SiC layer while it is in tension itself, as observed experimentally here. SiC is deposited at  $\sim 200^\circ\text{C}$  higher temperature than PyC, thus the IPyC layer has experienced a higher temperature during manufacturing than the OPyC layer which may result in different properties.

The thermal expansion coefficients of the exact forms of SiC and PyC in TRISO coatings is unknown, however  $4.4 \times 10^{-6} \text{ K}^{-1}$  is generally accepted as a single value for cubic CVD SiC between room temperature and  $1000^\circ\text{C}$ , but varies as a function of temperature between  $2.17 \times 10^{-6} \text{ K}^{-1}$  and  $4.63 \times 10^{-6} \text{ K}^{-1}$  at  $1700^\circ\text{C}$  [18]. The thermal expansion coefficient for pyrolytic carbon is especially uncertain, being calculated in

the range  $6\text{--}8 \times 10^{-6} \text{ K}^{-1}$  for perfectly isotropic carbon [66], and experimentally found as  $5.5 \times 10^{-6} \text{ K}^{-1}$  [18]. These values give a differential thermal expansion coefficient between 1.1 and  $5.8 \times 10^{-6} \text{ K}^{-1}$ , larger than the  $0.5 \times 10^{-6} \text{ K}^{-1}$  used in reference [10] and correspondingly increasing the residual stresses from those calculated. Additionally, the Young's modulus for PyC in reference [10] is lower than measured here, while for SiC it is larger.

Applying a simple differential expansion force balance calculation to the UNSC particle, with  $6.75 \times 10^{-6} \text{ K}^{-1}$  for the thermal expansion coefficient of PyC, and  $4.4 \times 10^{-6} \text{ K}^{-1}$  for SiC cooling from  $1500^\circ\text{C}$  to room temperature gives a residual tangential stress of  $-187 \text{ MPa}$  in SiC, and  $110 \text{ MPa}$  in PyC. The estimate for the PyC stress is in the range of that experimentally measured in this work, in fact slightly higher due to porosity or cracking during cooling which is not captured in this estimate. The estimated value for SiC is considerably lower than measured. This may imply that compressive stresses were already introduced to the polycrystalline SiC layer during CVD growth. Cooling down from high temperature further enhanced the stress level. The FEA modelling of cross-sectioning shows a factor of two difference in the stress in SiC when the boundary condition is removed which may further add to the discrepancy between the measured and predicted values.

The additional processing steps in incorporating a TRISO particle into a SiC or graphite matrix may also modify the stress state and the physical or mechanical properties of the TRISO coatings. This could be during the graphitisation (or annealing) heat treatments in the case of graphite pebbles and pellets, or during sintering shrinkage in the case of hot-pressed SiC pellets [67,68]. The fuel matrix will also affect stresses in particle coatings during service. Boer *et al.* calculated that service stresses in TRISO coatings are different when incorporated into a graphite matrix, depending on the dimensional change (shrinkage and swelling) and the creep coefficient of the particular form of graphite [14]. During graphite shrinkage, compressive stress is applied to the TRISO particles, which is beneficial for particle integrity, however at higher neutron fluences graphite swelling applies tensile stresses to TRISO coatings leading to earlier failure than for a free-standing particle assuming there is a mechanical connection between the OPyC layer and the matrix material. Proximity to neighbouring particles, and the packing orientation also influence stresses in TRISO particles [14,69]. As silicon carbide undergoes radiation swelling, TRISO particles in a SiC matrix are likely to experience additional tensile stresses compared to isolated TRISO particles. This may depend on any protective overcoating which has been applied to the TRISO particles during fuel pellet manufacturing, and the strength of the particle–matrix interface. It is therefore important to study TRISO particles while they are incorporated in their matrices; deconsolidated particles are likely to be in a different state to those embedded in a matrix.

#### 4.2. Practical considerations for FIB-DIC of TRISO

Stress redistribution during sectioning a stressed coated particle can change the measurements of residual stress, or indeed other mechanical or structural properties of the coatings. Most significantly, tensile stresses near interfaces may cause interfacial cracking and further stress changes. The origin of residual stresses in the finite element models here is typically the thermal expansion mismatch of the surrogate kernels. In previous peridynamic modelling work, debonding was predicted between the kernel and buffer, therefore the values of predicted stress here are not representative [65]. Micrographs of TRISO particles in the literature occasionally show cracks at coating interfaces and circumferential cracks in the SiC layer, which is sometimes attributed to poor edge retention during sample preparation due to the large difference in hardness between SiC and PyC materials [21,34]. This type of cracking could also be related to stress redistribution during cross-sectioning if the sample mounting is compliant, or there are shrinkage gaps between the mounting resin and the sample. Terrani *et al.* observed a circumferential crack around the entire SiC layer of a cross section of a

prototype UN TRISO particle irradiated at  $460^\circ\text{C}$  with a fast neutron fluence of  $\sim 3.2 \times 10^{20} \text{ n/cm}^2$  [70]. Radial stresses to generate this crack were not predicted to occur based on fuel performance modelling; they may instead be related to a redistribution of residual stresses as predicted here and an increase in stress intensity factor at pores in the SiC layer. The observation of interfacial cracks in the sample prepared by non-contact laser milling suggests that stress redistribution is the primary cause of interfacial or circumferential cracking, rather than mechanical preparation itself. The mechanically prepared TRISO particle embedded in a stiff SiC matrix does not have signs of interfacial debonding, showing that suitable sample mounting is vital for studying cross-sections of TRISO particles. Although sample mounting is critical, this was not predicted to fully solve the issue of stress redistribution by hemisectioning a spherical particle. The fact remains that measurements made on a cross-sectioned TRISO particle are likely to be different to the properties of a complete spherical particle.

As discussed, the *y*-direction is less reliable for SEM-DIC experiments due to being the slow scanning direction of the electron beam, despite the image averaging and short dwell time used in this work. Future experiments are planned to improve this by rotating the SEM scan direction during the imaging step, and by repeating on several pillars at different orientations. This will also improve the reliability of residual stress measurements.

Further work will involve measuring stresses in irradiated surrogate particles to investigate the role of irradiation induced shrinkage and creep of PyC, and defect swelling of SiC. As this FIB-DIC method does not measure spacing of crystal planes like diffraction or chemical bonding as spectroscopy does, these experiments can be conducted on samples post irradiation with no degradation to the measurement. Irradiated surrogates are a useful way of isolating the material response and separating complex nuclear effects, giving valuable material properties for fuel performance modelling. Coated fuel particles containing a real fuelled kernel will behave differently during service due to dimensional swelling of the kernel as uranium fissions and various solid and gaseous products are produced. Cross sectioning a particle necessarily relieves any internal fission gas pressure, so the full stress state of an ex-reactor fuel particle cannot be investigated. Nevertheless, these measurements could give vital insight into the evolution of TRISO coating properties in a reactor environment.

## 5. Conclusions

This paper has identified the need for measuring residual stresses in coated fuel particles and demonstrated ring-core FIB-DIC as a potential method for measuring these. Further development of the method, including modelling work, would be beneficial to improve its reliability and quantification of the results.

The process of cross sectioning a particle for analysis inherently alters the stress state of the particle by allowing relaxation radially, as well as perpendicular to the cut surface; it is not a simple plane-stress state. Further technique development is required to account for this, whether by constraining the particle in a stiff matrix as attempted here, or by applying a mathematical correction derived from modelling. The finite element modelling performed here illustrates that stress is redistributed by cross-sectioning particles, therefore properties measured on a cross-section may not be wholly comparable to properties of a complete spherical particle.

In the as-processed condition, the silicon carbide layer experiences a compressive residual hoop stress while pyrolytic carbon experiences a tensile hoop stress. This is consistent with larger thermal shrinkage of PyC during cooling from the manufacturing temperature. The compressive stress in SiC is beneficial in opposing stresses leading to radial cracks through the TRISO coatings, increasing the safety margin, or extending the lifetime of these particles. These observations could be used to improve fuel performance modelling of TRISO particles, improving their reliability in operation. These measurements can also be

used to inform processing conditions which may be optimised to improve the residual stress levels in TRISO coatings, in conjunction with incorporating particles into a graphite or SiC matrix.

### CRedit authorship contribution statement

**Alexander J. Leide:** Conceptualization, Methodology, Software, Formal analysis, Investigation, Data curation, Writing – original draft, Visualization. **Thomas A. Haynes:** Formal analysis, Visualization, Investigation, Writing – review & editing. **Nassia Tzelepi:** Writing – review & editing. **John Payne:** Formal analysis, Visualization, Investigation. **Matthew Jordan:** . **Steven Knol:** Resources. **Jan A. Vreeling:** Resources. **Mark Davies:** Resources, Supervision. **David T. Goddard:** Conceptualization, Writing – review & editing, Supervision, Funding acquisition, Project administration. **Manuel J. Pfeifenberger:** Investigation. **Markus Alfreider:** Investigation. **Daniel Kiener:** Writing – review & editing, Resources, Funding acquisition. **Dong Liu:** Conceptualization, Validation, Resources, Funding acquisition, Writing – review & editing, Supervision, Project administration, Visualization.

### Declaration of Competing Interest

The authors declare that they have no known competing financial interests or personal relationships that could have appeared to influence the work reported in this paper.

### Data availability

Data will be made available on request.

### Acknowledgements

This research was funded under the £46 m Advanced Fuel Cycle Programme as part of the Department for Business, Energy, and Industrial Strategy's (BEIS) £505 m Energy Innovation Programme. The authors gratefully thank Prof Marco Sebastiani and Dr Edoardo Rossi for helpful discussions on the FIB-DIC measurement method. DK acknowledges financial support from the European Research Council under Grant Number 771146 (TOUGHIT). This project was supported by the Royal Academy of Engineering under the Research Fellowship programme.

### Appendix A. Supplementary material

Supplementary data to this article can be found online at <https://doi.org/10.1016/j.nme.2023.101470>.

### References

- [1] M.S.T. Price, The dragon project origins, achievements and legacies, *Nucl. Eng. Des.* 251 (2012) 60–68, <https://doi.org/10.1016/j.nucengdes.2011.12.024>.
- [2] O.M. Stansfield, Evolution of HTGR coated particle fuel design, *Energy*. 16 (1991) 33–45, [https://doi.org/10.1016/0360-5442\(91\)90085-Z](https://doi.org/10.1016/0360-5442(91)90085-Z).
- [3] R.L. Seibert, B.C. Jolly, M. Balooch, D.P. Schappel, K.A. Terrani, Production and characterization of TRISO fuel particles with multilayered SiC, *J. Nucl. Mater.* 515 (2019) 215–226, <https://doi.org/10.1016/j.jnucmat.2018.12.024>.
- [4] S. De Groot, P. Guillermier, K. Sawa, J.M. Esclaine, S. Ueta, V. Basini, K. Bakker, Y. W. Lee, M. Perez, B.G. Kim, HTR fuel coating separate effect test PYCASSO, *Nucl. Eng. Des.* 240 (2010) 2392–2400, <https://doi.org/10.1016/j.nucengdes.2010.05.052>.
- [5] K. Verfondern, H. Nabielek, J.M. Kendall, Coated Particle Fuel for High Temperature Gas Cooled Reactors, *Nucl. Eng. Technol.* 39 (5) (2007) 603–616, <https://doi.org/10.5516/NET.2007.39.5.603>.
- [6] T.J. Gerczak, J.D. Hunn, R.A. Lowden, T.R. Allen, SiC layer microstructure in AGR-1 and AGR-2 TRISO fuel particles and the influence of its variation on the effective diffusion of key fission products, *J. Nucl. Mater.* 480 (2016) 257–270, <https://doi.org/10.1016/j.jnucmat.2016.08.011>.
- [7] J.J. Powers, W.J. Lee, F. Venneri, L.L. Snead, C.K. Jo, D.H. Hwang, J.H. Chun, Y.H. Kim, K.A. Terrani, Fully Ceramic Microencapsulated (FCM) Replacement Fuel For LWRs, 2013.
- [8] G.K. Miller, D.A. Petti, D.J. Varacalle, J.T. Maki, Consideration of the effects on fuel particle behavior from shrinkage cracks in the inner pyrocarbon layer, *J. Nucl. Mater.* 295 (2001) 205–212, [https://doi.org/10.1016/S0022-3115\(01\)00551-7](https://doi.org/10.1016/S0022-3115(01)00551-7).
- [9] G.K. Miller, D.A. Petti, J.T. Maki, Consideration of the effects of partial debonding of the IPyC and particle asphericity on TRISO-coated fuel behavior, *J. Nucl. Mater.* 334 (2004) 79–89, <https://doi.org/10.1016/j.jnucmat.2004.04.330>.
- [10] D.G. Martin, Considerations pertaining to the achievement of high burn-ups in HTR fuel, *Nucl. Eng. Des.* 213 (2002) 241–258, [https://doi.org/10.1016/S0029-5493\(01\)00502-7](https://doi.org/10.1016/S0029-5493(01)00502-7).
- [11] J.J. Powers, B.D. Wirth, A review of TRISO fuel performance models, *J. Nucl. Mater.* 405 (2010) 74–82, <https://doi.org/10.1016/j.jnucmat.2010.07.030>.
- [12] R. Li, B. Liu, K. Verfondern, The study of irradiation-induced failure behavior for the TRISO-coated fuel particle in HTGR, *J. Nucl. Mater.* 516 (2019) 214–227, <https://doi.org/10.1016/j.jnucmat.2019.01.029>.
- [13] W.F. Skerjanc, J.T. Maki, B.P. Collin, D.A. Petti, Evaluation of design parameters for TRISO-coated fuel particles to establish manufacturing critical limits using PARFUME, *J. Nucl. Mater.* 469 (2016) 99–105, <https://doi.org/10.1016/j.jnucmat.2015.11.027>.
- [14] B. Boer, A.M. Ougouag, J.L. Kloosterman, G.K. Miller, Stress Analysis of Coated Particle Fuel in Graphite of High-Temperature Reactors, *Nucl. Technol.* 162 (2008) 276–292, <https://doi.org/10.13182/NT08-A3956>.
- [15] R. Li, B. Liu, C. Tang, Sensitivity of stresses in TRISO-coated fuel particles to the coating layer properties, *Nucl. Eng. Des.* 307 (2016) 309–318, <https://doi.org/10.1016/j.nucengdes.2016.07.010>.
- [16] G.K. Miller, Stresses in a spherical pressure vessel undergoing creep and dimensional changes, *Int. J. Solids Struct.* 32 (1995) 2077–2093, [https://doi.org/10.1016/0020-7683\(94\)00197-5](https://doi.org/10.1016/0020-7683(94)00197-5).
- [17] T.S. Byun, J.D. Hunn, J.H. Miller, L.L. Snead, J.W. Kim, Evaluation of fracture stress for the SiC layer of TRISO-coated fuel particles using a modified crush test method, *Int. J. Appl. Ceram. Technol.* 7 (2010) 327–337, <https://doi.org/10.1111/j.1744-7402.2009.02462.x>.
- [18] L.L. Snead, T. Nozawa, Y. Katoh, T.-S. Byun, S. Kondo, D.A. Petti, Handbook of SiC properties for fuel performance modeling, *J. Nucl. Mater.* 371 (2007) 329–377, <https://doi.org/10.1016/j.jnucmat.2007.05.016>.
- [19] G.K. Miller, D.A. Petti, D.J. Varacalle, J.T. Maki, Statistical approach and benchmarking for modeling of multi-dimensional behavior in TRISO-coated fuel particles, *J. Nucl. Mater.* 317 (1) (2003) 69–82, [https://doi.org/10.1016/S0022-3115\(02\)01702-6](https://doi.org/10.1016/S0022-3115(02)01702-6).
- [20] N. Rohbeck, D. Tsvoulas, I.P. Shapiro, P. Xiao, S. Knol, J.M. Esclaine, M. Perez, B. Liu, Comparison study of silicon carbide coatings produced at different deposition conditions with use of high temperature nanoindentation, *J. Mater. Sci.* 52 (2017) 1868–1882, <https://doi.org/10.1007/s10853-016-0476-5>.
- [21] P. Hosemann, J.N. Martos, D. Frazer, G. Vasudevamurthy, T.S. Byun, J.D. Hunn, B. C. Jolly, K. Terrani, M. Okuniewski, Mechanical characteristics of SiC coating layer in TRISO fuel particles, *J. Nucl. Mater.* 442 (2013) 133–142, <https://doi.org/10.1016/j.jnucmat.2013.08.041>.
- [22] D.G. Martin, An analysis of stresses created in the layers of coated fuel particles by temperature changes, in: *Int. Conf. Struct. Mech. React. Technol.*, IASMiRT, London, 1975: pp. 1–9.
- [23] D. Liu, S. Knol, J. Ell, H. Barnard, M. Davies, J.A. Vreeling, R.O. Ritchie, X-ray tomography study on the crushing strength and irradiation behaviour of dedicated tristructural isotropic nuclear fuel particles at 1000 °C, *Mater. Des.* 187 (2020), 108382, <https://doi.org/10.1016/j.matdes.2019.108382>.
- [24] X. Zhao, R.M. Langford, J. Tan, P. Xiao, Mechanical properties of SiC coatings on spherical particles measured using the micro-beam method, *Scr. Mater.* 59 (2008) 39–42, <https://doi.org/10.1016/j.scriptamat.2008.02.022>.
- [25] N. Rohbeck, D. Tsvoulas, I.P. Shapiro, P. Xiao, S. Knol, J.M. Esclaine, M. Perez, In-situ nanoindentation of irradiated silicon carbide in TRISO particle fuel up to 500 °C, *J. Nucl. Mater.* 465 (2015) 692–694, <https://doi.org/10.1016/j.jnucmat.2015.06.035>.
- [26] G.T. Van Rooyen, R. Du Preez, J. De Villiers, R. Cromarty, The fracture strength of TRISO-coated particles determined by compression testing between soft aluminium anvils, *J. Nucl. Mater.* 403 (2010) 126–134, <https://doi.org/10.1016/j.jnucmat.2010.06.011>.
- [27] K.E. Gilchrist, J.E. Brocklehurst, A technique for measuring the strength of high temperature reactor fuel particle coatings, *J. Nucl. Mater.* 43 (1972) 347–350, [https://doi.org/10.1016/0022-3115\(72\)90069-4](https://doi.org/10.1016/0022-3115(72)90069-4).
- [28] A. Briggs, R.W. Davidge, C. Padgett, S. Quickenden, Crushing behaviour of high temperature reactor coated fuel particles, *J. Nucl. Mater.* 61 (1976) 233–242, [https://doi.org/10.1016/0022-3115\(76\)90262-2](https://doi.org/10.1016/0022-3115(76)90262-2).
- [29] R.D. Cromarty, G.T. Van Rooyen, J.P.R. De Villiers, Crush strength of silicon carbide coated TRISO particles: Influence of test method and process variables, *J. Nucl. Mater.* 445 (2014) 30–36, <https://doi.org/10.1016/j.jnucmat.2013.10.041>.
- [30] K. Minato, K. Fukuda, K. Ikawa, H. Matsushima, S. Kurobane, Crushing strength of irradiated Triso coated fuel particles, *J. Nucl. Mater.* 119 (1983) 326–332, [https://doi.org/10.1016/0022-3115\(83\)90211-8](https://doi.org/10.1016/0022-3115(83)90211-8).
- [31] T. Ogawa, K. Ikawa, Crushing strengths of SiC-Triso and ZrC-Triso coated fuel particles, *J. Nucl. Mater.* 98 (1981) 18–26, [https://doi.org/10.1016/0022-3115\(81\)90383-4](https://doi.org/10.1016/0022-3115(81)90383-4).
- [32] A.J. Leide, R.I. Todd, D.E.J. Armstrong, Effect of Ion Irradiation on Nanoindentation Fracture and Deformation in Silicon Carbide, *Jom.* 73 (2021) 1617–1628, <https://doi.org/10.1007/s11837-021-04636-8>.
- [33] L. Tan, T.R. Allen, J.D. Hunn, J.H. Miller, EBSD for microstructure and property characterization of the SiC-coating in TRISO fuel particles, *J. Nucl. Mater.* 372 (2008) 400–404, <https://doi.org/10.1016/j.jnucmat.2007.04.048>.

- [34] R. Kirchhofer, J.D. Hunn, P.A. Demkowicz, J.I. Cole, B.P. Gorman, Microstructure of TRISO coated particles from the AGR-1 experiment: SiC grain size and grain boundary character, *J. Nucl. Mater.* 432 (2013) 127–134, <https://doi.org/10.1016/j.jnucmat.2012.08.052>.
- [35] R. Kirchhofer, B. Hansford, I. Reimanis, B. Gorman, Characterization of Stresses in the SiC Layer of TRISO Coated Nuclear Fuels Using Raman Spectroscopy and EBSD, *Microsc. Microanal.* 16 (2010) 1616–1617, <https://doi.org/10.1017/S1431927610058770>.
- [36] P.J. Withers, H.K.D.H. Bhadeshia, Residual stress part 1 - Measurement techniques, *Mater. Sci. Technol.* 17 (2001) 355–365, <https://doi.org/10.1179/026708301101509980>.
- [37] J. Guo, H. Fu, B. Pan, R. Kang, Recent progress of residual stress measurement methods: A review, *Chinese J. Aeronaut.* 34 (2020) 54–78, <https://doi.org/10.1016/j.cja.2019.10.010>.
- [38] J.F. DiGregorio, T.E. Furtak, Analysis of Residual Stress in 6H-SiC Particles within Al<sub>2</sub>O<sub>3</sub>/SiC Composites through Raman Spectroscopy, *J. Am. Ceram. Soc.* 75 (1992) 1854–1857, <https://doi.org/10.1111/j.1151-2916.1992.tb07207.x>.
- [39] C.A. Taylor, M.F. Wayne, W.K.S. Chiu, Residual stress measurement in thin carbon films by Raman spectroscopy and nanoindentation, *Thin Solid Films.* 429 (2003) 190–200, [https://doi.org/10.1016/S0040-6090\(03\)00276-1](https://doi.org/10.1016/S0040-6090(03)00276-1).
- [40] O. Frank, G. Tsoukleri, I. Riaz, K. Papagelis, J. Parthenios, A.C. Ferrari, A.K. Geim, K.S. Novoselov, C. Galiotis, Development of a universal stress sensor for graphene and carbon fibres, *Nat. Commun.* 2 (2011) 255, <https://doi.org/10.1038/ncomms1247>.
- [41] R. Krishna, A.N. Jones, R. Edge, B.J. Marsden, Residual stress measurements in polycrystalline graphite with micro-Raman spectroscopy, *Radiat. Phys. Chem.* 111 (2015) 14–23, <https://doi.org/10.1016/j.radphyschem.2015.02.007>.
- [42] D. Ghosh, G. Subhash, N. Orlovskaya, Measurement of scratch-induced residual stress within SiC grains in ZrB<sub>2</sub>-SiC composite using micro-Raman spectroscopy, *Acta Mater.* 56 (2008) 5345–5354, <https://doi.org/10.1016/j.actamat.2008.07.031>.
- [43] D. Olego, M. Cardona, Pressure dependence of Raman phonons of Ge and 3C-SiC, *Phys. Rev. B.* 25 (1982) 1151–1160, <https://doi.org/10.1103/PhysRevB.25.1151>.
- [44] J.F. DiGregorio, T.E. Furtak, J.J. Petrovic, A Technique for Measuring Residual-Stress in SiC Whiskers within an Alumina Matrix through Raman-Spectroscopy, *J. Appl. Phys.* 71 (7) (1992) 3524–3531.
- [45] J. Liu, Y.K. Vohra, Raman Modes of 6H Polymorph of Silicon Carbide to Ultrahigh Pressures: A Comparison with Silicon and Diamond, *Phys. Rev. Lett.* 72 (1994) 4105–4108, <https://doi.org/10.1103/PhysRevLett.72.4105>.
- [46] T. Koyanagi, Y. Katoh, M.J. Lance, Raman spectroscopy of neutron irradiated silicon carbide: Correlation among Raman spectra, swelling, and irradiation temperature, *J. Raman Spectrosc.* 49 (2018) 1686–1692, <https://doi.org/10.1002/jrs.5425>.
- [47] A. Debelle, A. Boule, A. Chartier, F. Gao, W.J. Weber, Interplay between atomic disorder, lattice swelling, and defect energy in ion-irradiation-induced amorphization of SiC, *Phys. Rev. B.* 90 (2014), 174112, <https://doi.org/10.1103/PhysRevB.90.174112>.
- [48] A.J. Leide, *Reaction-bonded silicon carbide for nuclear fusion blanket applications*, University of Oxford, 2019.
- [49] A.J.G. Lunt, A.M. Korsunsky, A review of micro-scale focused ion beam milling and digital image correlation analysis for residual stress evaluation and error estimation, *Surf. Coat. Technol.* 283 (2015) 373–388, <https://doi.org/10.1016/j.surfcoat.2015.10.049>.
- [50] R. Schönggrundner, R. Treml, T. Antretter, D. Kozic, W. Ecker, D. Kiener, R. Brunner, Critical assessment of the determination of residual stress profiles in thin films by means of the ion beam layer removal method, *Thin Solid Films.* 564 (2014) 321–330, <https://doi.org/10.1016/j.tsf.2014.06.003>.
- [51] A.M. Korsunsky, M. Sebastiani, E. Bemporad, Residual stress evaluation at the micrometer scale: Analysis of thin coatings by FIB milling and digital image correlation, *Surf. Coat. Technol.* 205 (2010) 2393–2403, <https://doi.org/10.1016/j.surfcoat.2010.09.033>.
- [52] A.J.G. Lunt, E. Salvati, L. Ma, I.P. Dolbina, T.K. Neo, A.M. Korsunsky, Full in-plane strain tensor analysis using the microscale ring-core FIB milling and DIC approach, *J. Mech. Phys. Solids.* 94 (2016) 47–67, <https://doi.org/10.1016/j.jmps.2016.03.013>.
- [53] B. Winiarski, P.J. Withers, Micron-Scale Residual Stress Measurement by Micro-Hole Drilling and Digital Image Correlation, *Exp. Mech.* 52 (2012) 417–428, <https://doi.org/10.1007/s11340-011-9502-3>.
- [54] N. Sabaté, D. Vogel, A. Gollhardt, J. Keller, C. Cané, I. Gracia, J.R. Morante, B. Michel, Measurement of residual stress by slot milling with focused ion-beam equipment, *J. Micromech. Microeng.* 16 (2006) 254–259, <https://doi.org/10.1088/0960-1317/16/2/009>.
- [55] M. Sebastiani, C. Eberl, E. Bemporad, A.M. Korsunsky, W.D. Nix, F. Carassiti, Focused ion beam four-slot milling for Poisson's ratio and residual stress evaluation at the micron scale, *Surf. Coatings Technol.* 251 (2014) 151–161, <https://doi.org/10.1016/j.surfcoat.2014.04.019>.
- [56] S. Massl, H. Köstenbauer, J. Keckes, R. Pippan, Stress measurement in thin films with the ion beam layer removal method: Influence of experimental errors and parameters, *Thin Solid Films.* 516 (2008) 8655–8662, <https://doi.org/10.1016/j.tsf.2008.06.091>.
- [57] E. Salvati, T. Sui, A.M. Korsunsky, Uncertainty quantification of residual stress evaluation by the FIB-DIC ring-core method due to elastic anisotropy effects, *Int. J. Solids Struct.* 87 (2016) 61–69, <https://doi.org/10.1016/j.ijsolstr.2016.02.031>.
- [58] X. Song, K.B. Yeap, J. Zhu, J. Belnoue, M. Sebastiani, E. Bemporad, K.Y. Zeng, A. M. Korsunsky, Residual stress measurement in thin films using the semi-destructive ring-core drilling method using Focused Ion Beam, *Procedia Eng.* 10 (2011) 2190–2195, <https://doi.org/10.1016/j.proeng.2011.04.362>.
- [59] M.J. Pfeifenberger, M. Mangang, S. Wurster, J. Reiser, A. Hohenwarter, W. Pfleging, D. Kiener, R. Pippan, The use of femtosecond laser ablation as a novel tool for rapid micro-mechanical sample preparation, *Mater. Des.* 121 (2017) 109–118, <https://doi.org/10.1016/j.matdes.2017.02.012>.
- [60] A. Jelinek, M.J. Pfeifenberger, R. Pippan, D. Kiener, A Perspective to Control Laser-Induced Periodic Surface Structure Formation at Glancing-Incident Femtosecond Laser-Processed Surfaces, *Jom.* 73 (2021) 4248–4257, <https://doi.org/10.1007/s11837-021-04963-w>.
- [61] A.D. Kammers, S. Daly, Small-scale patterning methods for digital image correlation under scanning electron microscopy, *Meas. Sci. Technol.* 22 (2011), <https://doi.org/10.1088/0957-0233/22/12/125501>.
- [62] J. Blaber, B. Adair, A. Antoniou, Ncorr: Open-Source 2D Digital Image Correlation Matlab Software, *Exp. Mech.* 55 (2015) 1105–1122, <https://doi.org/10.1007/s11340-015-0009-1>.
- [63] W.C. Oliver, G.M. Pharr, Measurement of hardness and elastic modulus by instrumented indentation: Advances in understanding and refinements to methodology, *J. Mater. Res.* 19 (2004) 3–20, <https://doi.org/10.1557/jmr.2004.19.1.3>.
- [64] P. Pagliaro, M.B. Prime, J.S. Robinson, B. Clausen, Measuring Inaccessible Residual Stresses Using Multiple Methods and Superposition, (2011) 1123–1134. <https://doi.org/10.1007/s11340-010-9424-5>.
- [65] T.A. Haynes, A. Battistini, A.J. Leide, D. Liu, L. Jones, D. Shepherd, M.R. Wenman, Peridynamic modelling of cracking in TRISO particles for high temperature reactors, *J. Nucl. Mater.* 576 (2023), 154283, <https://doi.org/10.1016/j.jnucmat.2023.154283>.
- [66] R. Piat, E. Schnack, Modeling the effect of microstructure on the coefficients of the thermal expansion of pyrolytic carbon, *Carbon N. Y.* 41 (2003) 2162–2165, [https://doi.org/10.1016/S0008-6223\(03\)00231-8](https://doi.org/10.1016/S0008-6223(03)00231-8).
- [67] H.-G. Lee, D. Kim, S.J. Lee, J.Y. Park, W.-J. Kim, Distribution Analysis of TRISO-Coated Particles in Fully Ceramic Microencapsulated Fuel Composites, *J. Korean Ceram. Soc.* 55 (2018) 400–405, <https://doi.org/10.4191/kcers.2018.55.4.08>.
- [68] C. Ang, G. Singh, L. Snead, Y. Katoh, Preliminary study of sintering zero-rupture Fully Ceramic Microencapsulated (FCM) fuel, *Int. J. Appl. Ceram. Technol.* 16 (2019) 1699–1707, <https://doi.org/10.1111/ijac.13294>.
- [69] Y. Zhou, Z. Xiao, S. Liu, P. Chen, H. Pang, Y. Xin, Y. Jiao, S. Gao, K. Zhang, W. Li, J. Yu, Effect of structure on the thermal-mechanical performance of fully ceramic microencapsulated fuel, *Computation.* 8 (2020), <https://doi.org/10.3390/computation8010013>.
- [70] K.A. Terrani, B.C. Jolly, J.M. Harp, Uranium nitride tristructural-isotropic fuel particle, *J. Nucl. Mater.* 531 (2020), 152034, <https://doi.org/10.1016/j.jnucmat.2020.152034>.